ARTICLE

Curving the space by non-Hermiticity

Chenwei Lv [1,4], Ren Zhang[1,2,4], Zhengzheng Zhai[1] & Qi Zhou[1,3 ✉]

Quantum systems are often classified into Hermitian and non-Hermitian ones. Extraordinary non-Hermitian phenomena, ranging from the non-Hermitian skin effect to the super-sensitivity to boundary conditions, have been widely explored. Whereas these intriguing phenomena have been considered peculiar to non-Hermitian systems, we show that they can be naturally explained by a duality between non-Hermitian models in flat spaces and their counterparts, which could be Hermitian, in curved spaces. For instance, prototypical one-dimensional (1D) chains with uniform chiral tunnelings are equivalent to their duals in two-dimensional (2D) hyperbolic spaces with or without magnetic fields, and non-uniform tunnelings could further tailor local curvatures. Such a duality unfolds deep geometric roots of non-Hermitian phenomena, delivers an unprecedented routine connecting Hermitian and non-Hermitian physics, and gives rise to a theoretical perspective reformulating our under-standings of curvatures and distance. In practice, it provides experimentalists with a powerful two-fold application, using non-Hermiticity to engineer curvatures or implementing synthetic curved spaces to explore non-Hermitian quantum physics.

[1] Department of Physics and Astronomy, Purdue University, West Lafayette, IN 47907, USA. [2] School of Physics, Xi'an Jiaotong University, Xi'an, Shaanxi 710049, China. [3] Purdue Quantum Science and Engineering Institute, Purdue University, West Lafayette, IN 47907, USA. [4] These authors contributed equally: Chenwei Lv, Ren Zhang. ✉email: zhou753@purdue.edu

System-environment couplings lead to a plethora of intriguing non-Hermitian phenomena[1–9], such as non-orthogonal eigenstates, the non-Hermitian skin effect[10–16], real energy spectra in certain parameter regimes[17,18], collapsed energy spectra, and coalesced eigenstates at an exceptional point (EP)[12,19,20], and drastic responses to boundary conditions[21,22]. While these phenomena have been extensively explored in quantum sciences and technologies[2–5,8,23–27], peculiar theoretical tools are often required to study non-Hermitian physics. Though bi-orthogonal vectors and metric operators are introduced to restore orthogonality[11,19,28–30], the underlying physics of these mathematical tools is not clear yet. Moreover, it remains challenging to prove the real energy spectra of certain non-Hermitian systems, as the existence of the $\mathcal{PT}$ symmetry does not guarantee a real energy spectrum and sophisticated mathematical techniques are required[17,18,31].

In this work, we show a duality between non-Hermitian Hamiltonians in flat spaces and their counterparts in curved spaces. On the theoretical side, this duality leads to a geometric framework providing a unified explanation of several non-Hermitian phenomena. For instance, it is the finite curvature that requires an orthonormal condition distinct from that in flat spaces, enforces eigenstates to localize at edges, and gives rise to the supersensitivity to boundary conditions. Dual models in curved spaces could be Hermitian, providing a simple proof of the existence of real energy spectra in certain non-Hermitian systems. Moreover, in sharp contrast to existing schemes of studying curved spaces[32–35], which were built on the conventional wisdom that a flat space needs to be physically distorted to become curved, our results show that non-Hermiticity is a controllable knob for tuning curvatures even when the space appears to be flat, for instance, in lattices with fixed lattice spacing. This duality therefore may reform our understanding of distance and curvatures.
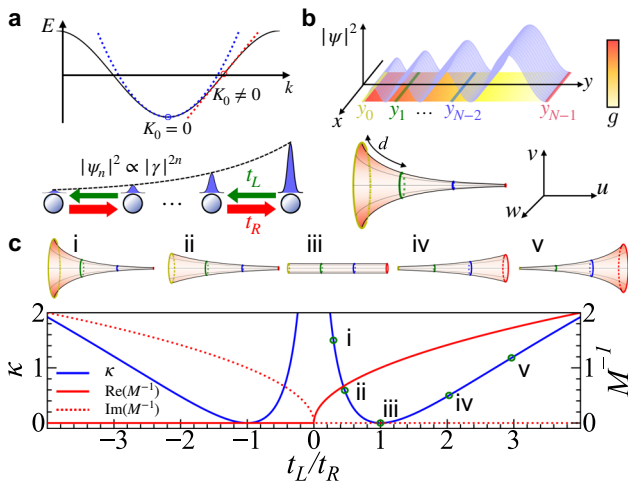

Fig. 1 The duality between the Hatano-Nelson (HN) model and a hyperbolic surface. a A HN chain and its energy spectrum as a function of k. Near a vanishing (finite) K_O, the effective theory in curved space is non-relativistic (relativistic). Eigenstates on the HN chain are localized at the edge, $|\psi_n|^2 \propto |\gamma|^{2n}$. **b** A HN chain is mapped to the shaded strip on the Poincaré half-plane, in which an eigenstate with $k_x = 0$ satisfies $|\psi|^2 \propto y$. This shaded strip on the Poincaré half-plane with PBC in the x-direction is equivalent to a pseudosphere embedded in 3D Euclidean space. **c** The curvature and the inverse of the effective mass, as functions of t_L for a fixed t_R. The unites of κ and M^{-1} are $1/d^2$ and $2t_R d^2/(\hbar^2)$, respectively. (i–v) show the dual pseudospheres of the HN model at various $t_L > 0$. A pseudosphere for $t_L < 0$ is the same as that for $-t_L$.

In practice, our duality has a two-fold implication. On the one hand, it establishes non-Hermiticity as a unique tool to simulate intriguing quantum systems in curved spaces. For instance, it offers an approach of using non-Hermitian systems in flat spaces to solve the grand challenge of accessing gravitational responses of quantum Hall states (QHS) in curved spaces[34,36–38]. On the other hand, the duality allows experimentalists to use curved spaces to explore non-Hermitian physics. Whereas a variety of non-Hermitian phenomena have been addressed in experiments, delicate designs of dissipations are often required[2,4,7–9,39–42]. Our results show that curved spaces can serve as an unprecedented means to explore non-Hermitian Hamiltonians without resorting to dissipations.

Results

Hatano-Nelson model and hyperbolic surfaces. Our duality can be demonstrated using the celebrated Hatano-Nelson (HN) model[43], which reads,

$$-t_R\psi_{n-1} - t_L\psi_{n+1} = E\psi_n, \qquad (1)$$

where $n = 0, 1, \ldots N-1$ is the lattice index of a one-dimensional (1D) chain, ψ_n is the eigenstate, E is the corresponding eigenenergy, and t_L and t_R are the nearest-neighbor tunneling amplitudes towards the left and the right, respectively. Under the open boundary condition (OBC), $\psi_0 = \psi_{N-1} = 0$, $\psi_n = e^{n\ln(\gamma)}\sin(k_m nd)/\sqrt{(N-1)/2}$, where $\gamma = \sqrt{t_R/t_L}$ characterizes the strength of non-Hermiticity, $k_m = m\pi/((N-1)d)$, $m = 1, 2, \ldots N-2$, and d is the lattice constant. The eigenenergy reads $E_m = -2\sqrt{t_L t_R}\cos(k_m d)$.

Similar to Hermitian lattice models, the effective theory of Eq. (1) in the continuum limit describes the motion of a non-relativistic (relativistic) particle at (away from) the band bottom and top, with a quadratic (linear) dispersion relation, as shown in Fig. 1a. At the band bottom, the effective theory is written as

$$-\frac{\hbar^2}{2M}\kappa\left(y^2\partial_y^2 + \frac{1}{4}\right)\psi(y) = E\psi(y), \qquad (2)$$

where $M = \hbar^2/(2\sqrt{t_L t_R}d^2)$ is the effective mass, and $\kappa = 4\ln^2(|\gamma|)/d^2$. Solutions to Eq. (2), $y^{\frac{1}{2}}y^{\pm ik_y/\sqrt{\kappa}}$, have the same energy, $\hbar^2 k_y^2/(2M)$. An eigenstate under OBC is their superposition, $\psi(y) = \sqrt{2/\ln(y_{N-1}/y_0)}(y/y_0)^{\frac{1}{2}}\sin\left[k_y\ln(y/y_0)/\sqrt{\kappa}\right]$ with $k_y = m\pi\sqrt{\kappa}/\ln(y_{N-1}/y_0)$ and $\psi(y_0) = \psi(y_{N-1}) = 0$. y_0 and y_{N-1} specify the positions of the two edges. At the band top, we have $M \to -M$. Eq. (2) is a dimension reduction of the Schrödinger equation on a Poincaré half-plane,

$$-\frac{\hbar^2}{2M}\kappa\left(y^2\nabla^2 + \frac{1}{4}\right)\Psi(x,y) = E\Psi(x,y), \qquad (3)$$

where $\nabla^2 \equiv \left(\partial_x^2 + \partial_y^2\right)$, $\Psi(x,y) = e^{ik_x x}\psi(y)$, and $-\kappa$ is the curvature (Supplementary Material). The metric tensor is $\mathbf{g} = \frac{1}{\kappa y^2}(\mathrm{d}x^2 + \mathrm{d}y^2)$, $g = \det(\mathbf{g}) = 1/(\kappa^2 y^4)$. Since k_x is a good quantum number, Eq. (3) reduces to Eq. (2) when $k_x = 0$. A finite k_x adds an onsite potential to the HN model,

$$V_n\psi_n - t_R\psi_{n-1} - t_L\psi_{n+1} = E\psi_n, \qquad (4)$$

where $V_n = a^2\sqrt{t_L t_R}\gamma^{4n}$. The dimensionless quantity $a^2 = 4(\ln^2|\gamma|)y_0^2 k_x^2$ characterizes the strength of V_n.

To derive the duality between the continuum limit of Eq. (1) at the band bottom and Eq. (2), we define $\psi_n \equiv \sqrt{d}\psi(s_n)$ with $s_n = nd$, such that the eigenstate of the HN model, ψ_n, defined on discrete lattice sites is extended to $\psi(s)$ as a function of a continuous variable s. Since ψ_n, under OBC, includes a part that

Table 1 The mapping between the continuum limit of the HN model near the band bottom under OBC and the Poincaré half-plane.

2D Hyperbolic surface	Curvature $-\kappa$	Energy scales $\hbar^2/(2Md^2)$	Coordinate $y_n = y_0 e^{n\sqrt{\kappa}d}$	Eigenfunctions $\psi(y) \propto (y/y_0)^{\frac{1}{2}} \sin\left(\frac{m\pi \ln(y/y_0)}{\ln(y_{N-1}/y_0)}\right)$	Eigenenergies $E_m = \frac{\kappa\hbar^2 m^2 \pi^2}{2M \ln(y_{N-1}/y_0)^2}$
1D Non-Hermitian chain	Non-Hermiticity $-4\ln^2(|\gamma|)/d^2$	Tunneling strength $\sqrt{t_R t_L}$	Lattice site n	$\psi_n \propto \gamma^n \sin(\frac{m\pi}{N-1}n)$	$\frac{E_m}{2\sqrt{t_R t_L}} = \left(-1 + \frac{m^2\pi^2}{2(N-1)^2} + O\left(\frac{m^4}{N^4}\right)\right)$

changes exponentially, i.e., $e^{n \ln(\gamma)}$, so does ψ. We thus define $\phi(s) \equiv \psi(s)e^{-qs}$ with $q = \ln(\gamma)/d = \frac{1}{2d}\ln(t_R/t_L)$ determining the inverse of the localization length, and $\phi(s)$ varies slowly with changing s. Then we have $\psi_n = \sqrt{d}\phi(s_n)e^{qs_n}$. Substituting ψ_n into Eq. (1) and using the Taylor expansion for $\phi(s)$, $\phi(s_{n\pm1}) = \phi(s_n) \pm d\partial_s\phi + \frac{1}{2}d^2\partial_s^2\phi$, we obtain $-\sqrt{t_L t_R}(2 + \partial_s^2)\phi = E\phi$. Consequently, $\psi(s)$ satisfies

$$-\sqrt{t_L t_R}d^2\left(\partial_s^2 - 2q\partial_s + q^2 + 2/d^2\right)\psi(s) = E\psi(s). \quad (5)$$

It describes a nonrelativistic particle subject to an imaginary vector potential, $A \sim iq$[39,43]. Unlike a real vector potential that amounts to a $U(1)$ gauge field, here, an imaginary vector potential curves the space. Performing a coordinate transformation $y/y_0 = e^{2qs}$ and applying $M = \hbar^2/(2\sqrt{t_L t_R}d^2)$, $\kappa = 4\ln^2(|\gamma|)/d^2$, we obtain Eq. (2) up to a constant energy shift $-2\sqrt{t_L t_R}$. The mapping between these two models is summarized in Table 1, which provides a dictionary translating microscopic parameters between them. For instance, ψ_n, the wavefunction at the n-th lattice site of the NH model is identical to $\psi(y_n)$, the wavefunction on the Poincaré half-plane evaluated at $y_n = y_0 e^{n\sqrt{\kappa}d}$. The low-energy limit of the eigenenergy of Eq. (1) is also identical to the eigenenergy of Eq. (2) as shown by Table 1.

Away from the band bottom(top), similar calculations can be performed by defining $\psi(s) = e^{\pm iK_0 s}e^{qs}\phi(s)$ using Taylor expansions of the slowly varying $\phi(s)$ and the same coordinate transformation $y = y_0 e^{2qs}$. We obtain the effective theory near $K_0 d \neq 0, \pm\pi$,

$$\left[E(K_0) \pm i\sqrt{\kappa}\hbar v_F y(\partial_y - 1/(2y))\right]\psi(y) = E\psi(y), \quad (6)$$

where $E(K_0) = -2\sqrt{t_L t_R}(\cos(K_0 d) + K_0 d \sin(K_0 d))$, $v_F = -2\sqrt{t_L t_R}d \sin(K_0 d)/\hbar$, and $\pm$ corresponds to the left and right moving waves centered near $\pm K_0$, respectively, The previously defined $\kappa = 4\ln^2(|\gamma|)/d^2$ has been used. The eigenstate under OBC includes both the left and right moving waves and is written as $\sqrt{2/\ln(y_{N-1}/y_0)}(y/y_0)^{\frac{1}{2}}\sin\left[k_y \ln(y/y_0)/\sqrt{\kappa}\right]$ with eigenenergy of $-2\sqrt{t_L t_R}[\cos(K_0 d) + (K_0 - k_y)d \sin(K_0 d)]$, which recovers the results of the HN model near a finite K_0.

Geometric interpretations of non-Hermitian phenomena. Our duality provides a natural explanation of several peculiar non-Hermitian phenomena. Firstly, the orthonormal condition of effective theories in Eq. (2) and Eq. (6) reads

$$\int \frac{dy}{\kappa y^2}\psi^*(y; k_y)\psi(y; k_y') = \mathcal{N}\delta_{k_y, k_y'}, \quad (7)$$

where the normalization constant $\mathcal{N}$ can be chosen freely. As a common feature of curved spaces, a finite curvature appears in the above equation. Considering a strip in the domain $x_0 \leq x \leq x_0 + L$, its width in the x-direction depends on y, $L_x(y) = \int_{x=x_0}^{x_0+L} dx/(\sqrt{\kappa}y) = L/(\sqrt{\kappa}y)$. Thus, a wave packet traveling in the y-direction must include an extra factor $y^{\frac{1}{2}}$ to guarantee the conservation of particle numbers. In the s-coordinate, Eq. (7) is written as $\int \frac{ds}{\sqrt{\kappa}y_0}e^{-2qs}\psi_{k_y}^*(s)\psi_{k_y'}(s) = \mathcal{N}\delta_{k_y, k_y'}$. Discretizing this

equation with $\mathcal{N} = (\sqrt{\kappa}y_0)^{-1}$, and transforming it to the HN model, we obtain,

$$\sum_n |\gamma|^{-2n}\psi_n^*(k_m)\psi_n(k_{m'}) = \delta_{k_m, k_{m'}}, \quad (8)$$

where $|\gamma|^{-2n}$ is precisely the difference between the left and right eigenvectors, or the metric operator[30]. The mapping to a curved space thus establishes an explicit physical interpretation of orthonormal conditions in non-Hermitian systems.

Secondly, the duality allows us to equate the non-Hermitian skin effect to its counterpart on the Poincaré half-plane we found recently[44]. This can be best visualized using the embedding of a hyperbolic surface in three-dimensional (3D) Euclidean space. We define $y = r_0 \cosh(\eta)$, $x = r_0\varphi$, where r_0 is an arbitrary constant and $\eta > 0$, $\varphi \in (-\pi, \pi)$. The embedding can then be written as

$$(u, v, w) = \frac{1}{\sqrt{\kappa}}\left((\eta - \tanh(\eta)), \frac{\cos(\varphi)}{\cosh(\eta)}, \frac{\sin(\varphi)}{\cosh(\eta)}\right). \quad (9)$$

This is a parameterization of a pseudosphere with a constant negative curvature and a radius of $1/\sqrt{\kappa}$, which satisfies $\left(u - \text{arcsech}(\sqrt{(v^2 + w^2)\kappa})/\sqrt{\kappa}\right)^2 + v^2 + w^2 = \kappa^{-1}$. As shown in Fig. 1b, a pseudosphere features a funnel shape, since the circumference of the circle with a fixed $y(\eta)$ changes with changing $y(\eta)$. As previously explained, a coordinate transformation $y = y_0 e^{2qs}$ maps eigenstates on the hyperbolic surface, $y^{\frac{1}{2}}y^{ik_y/\sqrt{\kappa}}$, to $e^{qs}e^{i(2q/\sqrt{\kappa})k_y s}$, which exponentially localizes near the funneling mouth, the smaller end.

Thirdly, the collapsed energy spectrum at EP of the HN models has a natural geometric interpretation. When $t_L = t_R$, the pseudosphere reduces to a cylinder with a vanishing κ. For a given $t_R(> t_L)$, κ increases with decreasing t_L. Increasing the non-Hermiticity thus makes the space more curved, as shown by Fig. 1 redc. Approaching EP, $t_L \to 0$, κ diverges, and the localization length, $1/\ln(|\gamma|)$, vanishes, forcing all eigenstates to coalesce. As eigenenergies read $E = \hbar^2 k_y^2/(2M)$ with divergent M, eigenenergies collapse to zero with a massive degeneracy. Across EP, $t_L t_R < 0$, and the effective mass becomes imaginary, all previous results of positive $t_L t_R$ still apply provided that $M \to \pm iM$. Particles moving in hyperbolic spaces are thus dissipative, and stationary states no longer exist.

Lastly, similar to the HN model, changing OBC to PBC leads to drastic changes in the curved space. Eigenstates of Eq. (2) and Eq. (6) normalized to $\mathcal{N}$ become $\sqrt{\kappa}\mathcal{N}(y_0^{-1} - y_{N-1}^{-1})^{-\frac{1}{2}}(y/y_0)^{ik_y/\sqrt{\kappa}}$, where $k_y = 2m\pi\sqrt{\kappa}/\ln(y_{N-1}/y_0))$ so that $\psi(y_0) = \psi(y_{N-1})$. Correspondingly, eigenenergies become complex. This can be explicitly shown from the time-dependent Schrödinger equations. For instance, at the band bottom(top), we multiply $\psi^*(y)$ to both sides of $i\hbar\partial_t\psi = -\frac{\hbar^2\kappa}{2M}\left(y^2\partial_y^2 + 1/4\right)\psi$, subtract from the resultant expression its complex conjugate, and integrate over y from y_0 to y_{N-1}. We find that the total particle number $\mathcal{N}_p = \int_{y_0}^{y_{N-1}} dy|\psi(y)|^2/(\kappa y^2)$ satisfies,

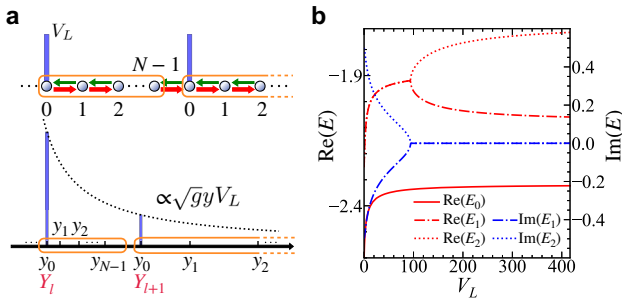$$\partial_t \mathcal{N}_p = \hbar\sqrt{\kappa}\mathcal{N}k_y/M, \quad (10)$$

Fig. 2 Changing boundary conditions. a A constant potential, V_L, is added to the first site in each unit cell of the superlattice. The corresponding potential in the curved space depends on the position. **b** Eigenenergies for the ground state $E_0 \in \mathbb{R}$ and the first two excited states $E_{1,2} \in \mathbb{C}$ as functions of V_L. $\sqrt{t_R/t_L} = 1.5$ and $N = 12$ are used.

which signifies the absence of a stationary state and explains complex eigenenergies under PBC. Using $\partial_t \mathcal{N}_p = \frac{2}{\hbar} \text{Im}(E) \mathcal{N}_p$, we find $\text{Im}(E) = \hbar^2 \sqrt{\kappa} k_y / (2M)$. This is distinct from the result for OBC, where $\psi(y) \sim y^{1/2} y^{\pm i k_y / \sqrt{\kappa}}$ such that $\partial_t \mathcal{N}_p = 0$. Similar calculations can be performed for effective theories away from the band top (bottom), $i\hbar \partial_t \psi = \left[E(K_0) + i\sqrt{\kappa} \hbar v_F y \left(\partial_y - 1/(2y) \right) \right] \psi$. Straightforward calculations show that $\partial_t \mathcal{N}_p = -\sqrt{\kappa} v_F \mathcal{N}$, which explains the imaginary part of the eigenenergy, $\text{Im}(E) = -\sqrt{\kappa} \hbar v_F / 2$.

Despite that $y_0 \neq y_{N-1}$, these two edges of a hyperbolic surface can be identified in mathematics, since the solutions under PBC exist, as we previously discussed. In physical systems, such PBC can also be realized. In fact, the boundary condition can be continuously tuned. An onsite energy offset, $V_L \geq 0$, in one of the lattice sites of the HN model continuously changes PBC to OBC once V_L increase from 0 to ∞. We consider a superlattice of a lattice spacing of Nd, whose unit cell is a HN chain, as shown in Fig. 2a. Figure 2b shows eigenenergies as functions of V_L. Similarly, an external potential can be added to the Poincaré half-plane,

$$V_\delta = d V_L \sqrt{\kappa} y \sum_l \delta(y - Y_l), \tag{11}$$

where $Y_l = y_0 e^{Nl\sqrt{\kappa}d}$ is the lattice site of the superlattice. The y-dependent amplitude of the delta-functions guarantees the scale invariance and the equivalence between each section between Y_l and Y_{l+1}. With V_L increasing from zero to infinity, eigenstates evolve from those under PBC to the ones under OBC. $\int_{Y_l^-}^{Y_l^+} \sqrt{g} dy V_\delta \sim 1/\sqrt{\kappa}$ sets the energy scale of the potential, such that the larger the non-Hermiticity is, the more sensitive of the system is to the boundary condition.

Generalizations to long-range and non-uniform tunnelings. Whereas the HN model provides an illuminating example of the duality, applications of our approach to generic non-Hermitian models are straightforward. We consider

$$-\sum_{m=1}^{M} t_{Rm} \psi_{n-m} - \sum_{m=1}^{M} t_{Lm} \psi_{n+m} = E \psi_n, \tag{12}$$

where t_{Rm} and t_{Lm} are tunneling amplitudes from the $(n \mp m)$th to nth sites. An eigenstate under OBC in the bulk is written as $e^{iknd+qnd}$, where $kd \in [0, 2\pi]$ and q is real. Unlike the HN model, where $q = \ln(t_R/t_L)/(2d)$ is a constant, once beyond the nearest neighbor tunnelings exist, q becomes a function of k and defines the so-called generalized Brillouin zone (BZ) in the complex plane[10,15,27,45,46]. Near any point in the generalized BZ specified

by $K_0 d \in [0, 2\pi]$, we define $\psi(s) = e^{iK_0 s} e^{q(K_0)s} \phi(s)$, where $\phi(s)$ changes slowly as a function of s, corresponding to small deviations of the momentum in the continuum limit. Similar to discussions about the HN model, the effective theory can be formulated straightforwardly using $\phi(s_{n\pm 1}) = \phi(s_n) \pm d\partial_s \phi + \frac{1}{2} d^2 \partial_s^2 \phi$. The Schrödinger equation satisfied by $\psi(s)$ is written as

$$-\mathcal{B}(K_0)[\partial_s^2 - 2\mathcal{A}(K_0)\partial_s + \mathcal{C}(K_0)]\psi(s) = E\psi(s), \tag{13}$$

where $\mathcal{A}(K_0)$, $\mathcal{B}(K_0)$ and $\mathcal{C}(K_0)$ depend on K_0, as well as t_{Rm} and t_{Lm}. When only the nearest neighbor tunnelings exist, the above equation recovers Eq. (5) at $K_0 = 0$ and $\mathcal{A}(K_0)$ becomes real and reduces to a constant imaginary vector potential $\sim \ln(t_R/t_L)/(2d)$ that we have discussed in the HN model. In the most generic case, $\mathcal{A}(K_0)$ provides a complex vector potential, whose real part curves the space. Using a coordinate transformation $y = y_0 e^{2\mathcal{A}_R(K_0)s}$, where $\mathcal{A}_R(K_0)$ is the real part of $\mathcal{A}(K_0)$, a hyperbolic surface is thus obtained in the same manner as the HN model. The only difference is that κ now is written as $\kappa = 4\mathcal{A}_R^2$ and depends on K_0. Such K_0-dependent curvature provides a geometric interpretation for the generalized BZ. Explicit calculations for a model including the next-nearest-neighbor interaction are given in Supplementary Materials (Fig. S1).

Whereas uniform chiral tunnelings lead to a hyperbolic surface with a constant curvature, we could also consider non-Hermitian models with non-uniform tunnelings,

$$-t_{R,n-1} \psi_{n-1} - t_{L,n} \psi_{n+1} = E \psi_n, \tag{14}$$

which gives rise to inhomogeneous local curvatures. For slowly varying $t_{R,n}$ and $t_{L,n}$, we define $\bar{t}(s)$ and $\bar{\gamma}(s)$ such that $\bar{t}(nd) = \frac{2Md^2}{\hbar^2} \sqrt{t_{R,n} t_{L,n}}$ and $\bar{\gamma}(nd) = \sqrt{t_{R,n}/t_{L,n}}$. We introduce a slowly changing function $\phi(s) = e^{v(s)/2} \psi(s)$ with $v(s) = \frac{2}{d} \int_0^s \ln(\bar{\gamma}(s'))ds'$. This is a generalization of the uniform case, where $v(nd)$ reduces to a linear function of n, i.e., the previously discussed $n\ln(\gamma)$ in the HN model. Using the same procedure, we obtain the effective theory of Eq. (14). For instance, the non-relativistic theory is written as

$$\frac{\hbar^2}{2M} \left(-\frac{1}{\sqrt{g}} \partial_i g^{ij} \sqrt{g} \partial_j - \frac{\kappa}{4} + V_c \right) \Psi(x, y) = E \Psi(x, y), \tag{15}$$

where $g_{xx} = g_{yy} = \sqrt{g} = \bar{t}(s_y) e^{-\frac{4}{d} \int_0^{s_y} \ln(\bar{\gamma}(s'))ds'}$, $g_{xy} = g_{yx} = 0$, $V_c = \frac{\hbar^2}{2Md^2} \left(\frac{d}{2} \partial_s \ln \bar{\gamma}|_{s_y} - 2 \right) \bar{t}(s_y)$, and the position-dependent curvature is written as $\kappa(y) = \bar{t}(s_y) \left(4 \ln \bar{\gamma}^2(s_y) - 2d\partial_s \ln \bar{\gamma}|_{s_y} \right)/d^2$. In these expressions, s_y is obtained from $y - y_0 = \int_0^{s_y} ds' e^{\frac{2}{d} \int_0^{s'} \ln(\bar{\gamma}(s''))ds''}/\bar{t}(s')$. The constant κ of a hyperbolic surface is recovered when $t_{R,n}$ and $t_{L,n}$ are constants. Changing $t_{R,n}$ and $t_{L,n}$ then tunes local curvatures. For instance, when $t_{R,n} = \frac{\hbar^2}{2Md^2} e^{-\Theta(n-n^*)/(2n)}$, $t_{L,n} = \frac{\hbar^2}{2Md^2} e^{\Theta(n-n^*)/(2n)}$, where $\Theta(x)$ is the Heaviside step function, the curvature vanishes everywhere except at a particular location, i.e., $\kappa \sim \delta(y - y^*)$, where $y^* = y_0 + n^* d$.

In addition to one dimension, many non-Hermitian models in higher dimensions can be constructed based on the HN model. For instance, 1D HN chains can be assembled to access higher dimensional curved spaces. Whereas curved spaces in higher dimensions are, in general, more complex than those in two dimensions, inter-chain couplings can be engineered to access different higher dimensional curved spaces (see Fig. S2 of Supplementary Materials).
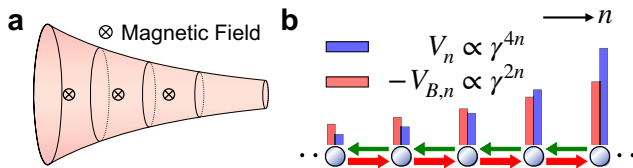
Fig. 3 Non-Hermitian realization of QHS on hyperbolic surface. a A hyperbolic surface threaded by uniform magnetic fluxes. **b** An extra onsite energy in HN chain, $V_{B,n}$, encapsulates the magnetic field.

Non-Hermitian realization of QHS in curved spaces. The duality we established has a wide range of profound applications. For instance, Fig. 3a shows a non-Hermitian realization of QHS in curved spaces. When a particle with a charge $-e$ is subjected to a uniform magnetic field, $y^2\nabla^2$ in Eq. (3) is replaced by $y^2[(\partial_x - i\frac{eB}{\hbar\kappa}\frac{1}{y})^2 + \partial_y^2]$, where we have chosen the gauge with the vector potential $\mathbf{A} = (-B/(\kappa y), 0)$[47] such that k_x is still a good quantum number. Wavefunctions of the lowest Landau level (LLL) are written as,

$$\psi_{\text{LLL}} = (2k_x)^{\frac{eB}{\hbar\kappa}-\frac{1}{2}}\sqrt{\frac{\mathcal{N}\kappa}{\Gamma(2\frac{eB}{\hbar\kappa}-1)L}}e^{-k_x y + ik_x x}y^{\frac{eB}{\hbar\kappa}}, \quad (16)$$

whose eigenenergies, $E_{LLL} = -\frac{\hbar^2\kappa}{8M} + \frac{\hbar eB}{2M}$, are independent of k_x, manifesting the degeneracy of the Landau levels. In the dual non-Hermitian systems, a finite magnetic field corresponds to an extra onsite potential in Eq. (4), $V_n \to V_n + V_{B,n}$, where $V_{B,n} = -ba\gamma^{2n}\sqrt{t_L t_R}$, as shown in Fig. 3b. The dimensionless b characterizing the strength of $V_{B,n}$ relative to V_n is written as

$$b = eBd^2/(\hbar\ln|\gamma|), \quad (17)$$

where $y_0 k_x = a(2\ln|\gamma|)^{-1}$ has been used. The magnetic flux density, $\rho_\phi = eB/(2\pi\hbar) = \frac{\ln|\gamma|}{2\pi d^2}b$, is thus determined by the ratio of $V_{B,n}$ to V_n. For a given B, a finite k_x shifts the position of the minimum of the total onsite potential $V_n + V_{B,n}$, similar to the well-known result of flat spaces where k_x determines the location of the minimum of the potential in the Landau gauge.

A complete description of QHS requires its gravitational responses in curved spaces. For instance, the particle density, ρ, depends on the local curvature[36],

$$\rho = \nu\rho_\phi - \kappa/(4\pi), \quad (18)$$

where ν is the filling factor. For integer QHS, $\nu = 1$ and Eq. (18) for a hyperbolic surface can be straightforwardly proved using Eq. (16) (Supplementary Materials). The counterpart of Eq. (18) in the non-Hermitian lattice is

$$|\gamma|^{2n}\int da \mathcal{N}_n(a,b) = b\ln(|\gamma|) - 2\ln^2(|\gamma|), \quad (19)$$

where $\mathcal{N}_n(a,b) = |\gamma|^{-2n}\psi_n^*\psi_n$ is the particle number at lattice site n in the non-Hermitian system. Mapping the magnetic flux, $eB/(2\pi\hbar)$, to the ratio between onsite potentials, $b\ln(|\gamma|)/(2\pi d^2)$, Eq. (18) and Eq. (19) are equivalent. The dependence of densities of QHS on curvatures is thus readily detectable using this non-Hermitian realization. An alternative scheme is to implement a 2D non-Hermitian lattice model as illustrated in Fig. S3 of Supplementary Materials, which serves as a non-Hermitian generalization of the Harper-Hofstadter Hamiltonian[48].

Discussion

In parallel to accessing curved spaces using non-Hermitian systems, experimentalists could also use curved spaces to study non-Hermitian physics[32,33,35]. In conventional understandings, non-Hermiticity arises when dissipations exist. While dissipations have been engineered in certain apparatuses to deliver desired non-Hermitian Hamiltonians[1,6,7], in other platforms, such engineering might be more difficult and sometimes experimentalists may have to use indirect means such as simulating non-Hermitian quantum walks[2,8,27]. Our results show that many non-Hermitian Hamiltonians are readily accessible using existing curved spaces. For instance, hyperbolic surfaces that have been created in laboratories could be used to realize the HN model directly. In particular, in contrast to current schemes used in the study of non-Hermitian physics, this method does not require engineering losses or gains. It thus provides a conceptually different protocol to access non-Hermiticity without dissipations.

The duality we have found provides insightful perspectives for both the studies of non-Hermitian physics and curved spaces. As the curvature depends on the non-Hermiticity even when the separation between any two points in the system is not physically distorted, our conventional understandings of distance may need to be reformed. We hope that our work will stimulate more interest in studying deep connections between non-Hermitian physics and curved spaces.

References
1. Syassen, N. et al. Strong dissipation inhibits losses and induces correlations in cold molecular gases. *Science* **320**, 1329 (2008).
2. Regensburger, A. et al. Parity–time synthetic photonic lattices. *Nature* **488**, 167 (2012).
3. Feng, L. et al. Single-mode laser by parity-time symmetry breaking. *Science* **346**, 972 (2014).
4. Longhi, S., Gatti, D. & Valle, G. D. Robust light transport in non-Hermitian photonic lattices. *Sci. Rep.* **5**, 13376 (2015).
5. Chen, W., Özdemir, Ş. K., Zhao, G., Wiersig, J. & Yang, L. Exceptional points enhance sensing in an optical microcavity. *Nature* **548**, 192 (2017).
6. Li, J. et al. Observation of parity-time symmetry breaking transitions in a dissipative Floquet system of ultracold atoms. *Nat. Commun.* **10**, 855 (2019).
7. Gou, W. et al. Tunable nonreciprocal quantum transport through a dissipative Aharonov-Bohm ring in ultracold atoms. *Phys. Rev. Lett.* **124**, 070402 (2020).
8. Weidemann, S. et al. Topological funneling of light. *Science* **368**, 311 (2020).
9. Helbig, T. et al. Generalized bulk–boundary correspondence in non-Hermitian topolectrical circuits. *Nat. Phys.* **16**, 747 (2020).
10. Yao, S. & Wang, Z. Edge states and topological invariants of non-Hermitian systems. *Phys. Rev. Lett.* **121**, 086803 (2018).
11. Kunst, F. K., Edvardsson, E., Budich, J. C. & Bergholtz, E. J. Biorthogonal bulk-boundary correspondence in non-Hermitian systems. *Phys. Rev. Lett.* **121**, 026808 (2018).
12. Martinez Alvarez, V. M., Barrios Vargas, J. E. & Foa Torres, L. E. F. Non-Hermitian robust edge states in one dimension: anomalous localization and eigenspace condensation at exceptional points. *Phys. Rev. B* **97**, 121401 (2018).
13. Lee, C. H. & Thomale, R. Anatomy of skin modes and topology in non-Hermitian systems. *Phys. Rev. B* **99**, 201103 (2019).
14. Borgnia, D. S., Kruchkov, A. J. & Slager, R.-J. Non-Hermitian boundary modes and topology. *Phys. Rev. Lett.* **124**, 056802 (2020).
15. Zhang, K., Yang, Z. & Fang, C. Correspondence between winding numbers and skin modes in non-Hermitian systems. *Phys. Rev. Lett.* **125**, 126402 (2020).
16. Okuma, N., Kawabata, K., Shiozaki, K. & Sato, M. Topological origin of non-Hermitian skin effects. *Phys. Rev. Lett.* **124**, 086801 (2020).
17. Bender, C. M. & Boettcher, S. Real spectra in non-Hermitian Hamiltonians having PT symmetry. *Phys. Rev. Lett.* **80**, 5243 (1998).

18. Mostafazadeh, A. Pseudo-hermiticity versus PT symmetry: The necessary condition for the reality of the spectrum of a non-Hermitian Hamiltonian. *J. Math. Phys.* **43**, 205 (2002).
19. Ashida, Y., Gong, Z. & Ueda, M. Non-Hermitian physics. *Adv. Phys.* **69**, 249 (2020).
20. Bergholtz, E. J., Budich, J. C. & Kunst, F. K. Exceptional topology of non-Hermitian systems. *Rev. Mod. Phys.* **93**, 015005 (2021).
21. Xiong, Y. Why does bulk boundary correspondence fail in some non-Hermitian topological models. *J. Phys. Commun.* **2**, 035043 (2018).
22. Okuma, N. & Sato, M. Topological phase transition driven by infinitesimal instability: majorana fermions in non-Hermitian spintronics. *Phys. Rev. Lett.* **123**, 097701 (2019).
23. Wiersig, J. Enhancing the sensitivity of frequency and energy splitting detection by using exceptional points: application to microcavity sensors for single-particle detection. *Phys. Rev. Lett.* **112**, 203901 (2014).
24. Kawabata, K., Shiozaki, K., Ueda, M. & Sato, M. Symmetry and topology in non-Hermitian physics. *Phys. Rev. X* **9**, 041015 (2019).
25. Lee, J. Y., Ahn, J., Zhou, H. & Vishwanath, A. Topological correspondence between Hermitian and non-Hermitian systems: anomalous dynamics. *Phys. Rev. Lett.* **123**, 206404 (2019).
26. Zhou, H. & Lee, J. Y. Periodic table for topological bands with non-Hermitian symmetries. *Phys. Rev. B* **99**, 235112 (2019).
27. Xiao, L. et al. Non-Hermitian bulk–boundary correspondence in quantum dynamics. *Nat. Phys.* **16**, 761 (2020).
28. Brody, D. C. Biorthogonal quantum mechanics. *J. Phys. A: Math. Theoretical* **47**, 035305 (2013).
29. Scholtz, F., Geyer, H. & Hahne, F. Quasi-Hermitian operators in quantum mechanics and the variational principle. *Ann. Phys.* **213**, 74 (1992).
30. Mostafazadeh, A. Pseudo-Hermitian representation of quantum mechanics. *Int. J. Geometric Methods Modern Phys.* **07**, 1191 (2010).
31. Dorey, P., Dunning, C. & Tateo, R. A reality proof in PT-symmetric quantum mechanics. *Czechoslovak J. Phys.* **54**, 35 (2004).
32. Bekenstein, R. et al. Control of light by curved space in nanophotonic structures. *Nat. Photon.* **11**, 664 (2017).
33. Zhou, X.-F. et al. Synthetic Landau levels and spinor vortex matter on a Haldane spherical surface with a magnetic monopole. *Phys. Rev. Lett.* **120**, 130402 (2018).
34. Schine, N., Chalupnik, M., Can, T., Gromov, A. & Simon, J. Electromagnetic and gravitational responses of photonic Landau levels. *Nature* **565**, 173 (2019).
35. Kollár, A. J., Fitzpatrick, M. & Houck, A. A. Hyperbolic lattices in circuit quantum electrodynamics. *Nature* **571**, 45 (2019).
36. Wen, X. G. & Zee, A. Shift and spin vector: new topological quantum numbers for the Hall fluids. *Phys. Rev. Lett.* **69**, 953 (1992).
37. Avron, J. E., Seiler, R. & Zograf, P. G. Viscosity of quantum Hall fluids. *Phys. Rev. Lett.* **75**, 697 (1995).
38. Can, T., Laskin, M. & Wiegmann, P. Fractional quantum Hall effect in a curved space: Gravitational anomaly and electromagnetic response. *Phys. Rev. Lett.* **113**, 046803 (2014).
39. Nelson, D. R. & Vinokur, V. M. Boson localization and correlated pinning of superconducting vortex arrays. *Phys. Rev. B* **48**, 13060 (1993).
40. Amir, A., Hatano, N. & Nelson, D. R. Non-Hermitian localization in biological networks. *Phys. Rev. E* **93**, 042310 (2016).
41. Lodahl, P. et al. Chiral quantum optics. *Nature* **541**, 473 (2017).
42. Yang, S.-H., Naaman, R., Paltiel, Y. & Parkin, S. S. P. Chiral spintronics. *Nat. Rev. Phys.* **3**, 328 (2021).
43. Hatano, N. & Nelson, D. R. Localization transitions in non-Hermitian quantum mechanics. *Phys. Rev. Lett.* **77**, 570 (1996).
44. Zhang, R., Lv, C., Yan, Y. & Zhou, Q. Efimov-like states and quantum funneling effects on synthetic hyperbolic surfaces. *Sci. Bull.* **66**, 1967 (2021).
45. Yokomizo, K. & Murakami, S. Non-Bloch band theory of non-Hermitian systems. *Phys. Rev. Lett.* **123**, 066404 (2019).
46. Yang, Z., Zhang, K., Fang, C. & Hu, J. Non-Hermitian bulk-boundary correspondence and auxiliary generalized Brillouin zone theory. *Phys. Rev. Lett.* **125**, 226402 (2020).
47. Comtet, A. On the Landau levels on the hyperbolic plane. *Ann. Phys.* **173**, 185 (1987).
48. Hofstadter, D. R. Energy levels and wave functions of Bloch electrons in rational and irrational magnetic fields. *Phys. Rev. B* **14**, 2239 (1976).

Author contributions
Q.Z. conceived the idea. C.L., R.Z., and Q.Z. performed analytical and numerical calculations with inputs from Z.Z. on parts of finite magnetic fields. Q.Z. wrote the manuscript with inputs from all authors.

Competing interests
The authors declare no competing interests.

Additional information
Supplementary information The online version contains supplementary material available at https://doi.org/10.1038/s41467-022-29774-8.

Correspondence and requests for materials should be addressed to Qi Zhou.

Peer review information *Nature Communications* thanks the other anonymous reviewer(s) for their contribution to the peer review of this work.

Reprints and permission information is available at http://www.nature.com/reprints

Publisher's note Springer Nature remains neutral with regard to jurisdictional claims in published maps and institutional affiliations.